Inorganic Chemistry
Article
Cite This: Inorg. Chem. 2018, 57, 11775−11781
pubs.acs.org/IC

# Controlled Crystal Growth of Indium Selenide, $In_2Se_3$, and the Crystal Structures of $\alpha$-$In_2Se_3$

Michael Küpers,[†] Philipp M. Konze,[†] Alexander Meledin,[‡,§] Joachim Mayer,[‡,§] Ulli Englert,[†] Matthias Wuttig,[∥,⊥,#] and Richard Dronskowski*[,†,#]

[†]Institute of Inorganic Chemistry and [‡]Central Facility for Electron Microscopy, RWTH Aachen University, 52056 Aachen, Germany
[§]Ernst Ruska-Centre for Microscopy and Spectroscopy with Electrons (ER-C), Forschungszentrum Jülich GmbH, 52428 Jülich, Germany
[∥]I. Institute of Physics, Physics of Novel Materials, RWTH Aachen University, 52056 Aachen, Germany
[⊥]JARA-Institute: Energy-Efficient Information Technology (Green IT), Forschungszentrum Jülich GmbH, 52428 Jülich, Germany
[#]Jülich-Aachen Research Alliance (JARA-FIT and JARA-HPC), RWTH Aachen University, 52056 Aachen, Germany

Supporting Information

**ABSTRACT:** $In_2Se_3$ has been known for over 100 years and recently attracted interest as a promising candidate for a variety of applications, such as solar cells, photodiodes, and phase-change memories. Despite the broad concern for possible uses, its polymorphism and structure are poorly characterized. By combining X-ray diffraction, transmission electron microscopy, and quantum-chemical calculations, we present here the crystal structures of two layered room-temperature polytypes: 3R and 2H $In_2Se_3$. Both polymorphs are stacking variants of the same Se−In−Se−In−Se layers comprising two coordination environments for the In atoms, one tetrahedral and one octahedral. By using chemical-bonding analysis, we look at the different In positions in $\alpha$-$In_2Se_3$ and compare them to those in the metastable $\beta$-phase.

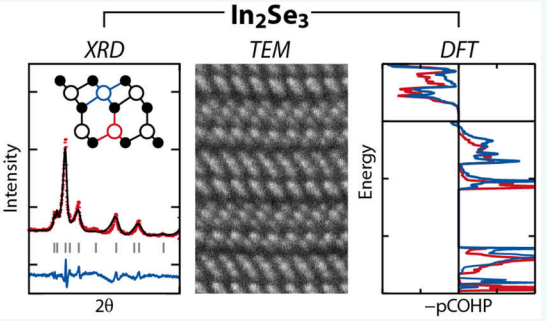


## INTRODUCTION

The archetypal phase $In_2Se_3$ is known for its outstanding photoelectric properties and possible applications in solar cells[1,2] or photodiodes.[3] Moreover, $In_2Se_3$ shows a plethora of other promising properties like thermo-[4−6] and ferroelectricity,[7−9] as well as a strong contrast in electrical properties between its different phases. Recently, the phase therefore gained interest as a phase-change material (PCM) for data storage.[10−12] Conventional PCMs switch between an amorphous and a crystalline state,[13] requiring the melting and also quenching of the material, which results in high stresses within the material and poor energy efficiency for the device. To achieve better performance, recent studies suggest the use of two different *crystalline* phases to store information. For layered compounds these unconventional PCMs have been dubbed interfacial PCMs (iPCM).[14]

Although $In_2Se_3$ is currently being discussed as a promising candidate for many applications, its crystal structures and the crystallization behavior of its polymorphs remain unclear, at best. Therefore, a thorough structural characterization of $In_2Se_3$ is of high interest, because it enables us to understand its physical properties and allows for the intelligent design of new data storage devices.

A compound with the $In_2Se_3$ stoichiometry has already been known since 1910[15] and was characterized by Klemm in 1934.[16] The polymorphism and phase diagram of $In_2Se_3$ are controversially discussed in the literature.[17−21] There are supposed to be at least four different polymorphs in the bulk material at ambient pressure: $\alpha$, $\beta$, $\gamma$, and $\delta$. In addition, $\alpha$-$In_2Se_3$ seemingly consists of two different stacking variants, the so-called 2H and 3R phases. High-pressure phase transitions starting from 3R $In_2Se_3$ were investigated very recently.[22] Concerning the crystal structures of $\alpha$-$In_2Se_3$, lots of different structure models are found in the literature,[4,9,23] where recently a model for the 2H phase was derived from electron microscopy,[24] but atomic parameters are, to the best of our knowledge, unknown.

In this work, we present, for the first time ever, a detailed structural characterization of the two $\alpha$-$In_2Se_3$ variants. The structural characterization using single-crystal and powder X-ray diffraction is complemented by high-resolution scanning transmission electron microscopy (HR STEM), as well as density-functional theory (DFT) calculations.

## METHODS

**Synthesis.** Samples of 3R $In_2Se_3$ were synthesized from the elements (In, HMW Hauner 99.999%; Se, MaTeck 99.999%) in

Received: July 12, 2018
Published: August 28, 2018






DOI: 10.1021/acs.inorgchem.8b01950
Inorg. Chem. 2018, 57, 11775−11781

evacuated quartz ampules. Samples were first heated to 500 °C within 1 h and then heated to 900 °C over the course of 20 h to prevent Se from evaporating too fast. The product was then held at 900 °C for 20 h and quickly cooled to room temperature.

Chemical transport[25,26] of $In_2Se_3$, using a temperature gradient from 800 to 700 °C and iodine (Merck 99.5%) as transport agent, resulted in very thin and brittle plate-like crystals of 2H $In_2Se_3$. Unfortunately, we were unable to isolate a single-crystalline specimen of the 2H crystals since they are mechanically very weak, and trying to cut or break larger crystals resulted in polycrystalline pieces.

**Characterization.** A sample tempered at 250 °C for 160 h and quenched to room temperature in air provided a twinned specimen of 3R $In_2Se_3$ with approximate dimensions of 0.05 × 0.05 × 0.01 $mm^3$. It was selected for a single-crystal diffraction experiment at room temperature, where 2018 reflections were collected in $\omega$ mode on a Bruker D8 goniometer equipped with an APEX CCD detector and an Incoatec microsource (Mo K$\alpha$ radiation, $\lambda$ = 0.71073 Å). Crystallographic and structure refinement data are shown in Table 1. The

**Table 1. Crystallographic and Structure Refinement Data of 3R $In_2Se_3$**

| | |
|---|---|
| formula | $In_2Se_3$ |
| formula weight (g/mol) | 466.52 |
| space group | *R*3*m* (No. 160) |
| *a* (Å) | 4.026(4) |
| *c* (Å) | 28.750(11) |
| *V* (Å$^3$) | 403.6(8) |
| *Z* | 3 |
| diffractometer | Bruker D8 goniometer with APEX CCD detector |
| Θ range | 2.125−28.602 |
| *hkl* ranges | $-4 \le h \le 4$; $-5 \le k \le 5$; $-37 \le l \le 37$ |
| no. reflns | 2018 |
| no. indep reflns | 310 |
| $R_{int}$ | 0.0639 |
| no. params | 20 |
| $R_1$; $wR_2$ (all data)[a] | 0.1084; 0.2444 |
| GOFt[a] | 1.097 |
| diffraction peak and hole (e Å$^{-3}$)[a] | 5.472/−8.642 |
| CCDC number | 1855522 |

[a]High residual parameters are explained in the text.

diffraction pattern was interpreted with the help of CELL_NOW:[27] 346 out of a subset of 379 reflections could be indexed when two domains with the lattice parameters for 3R $In_2Se_3$ known from powder diffraction were taken into account. The relationship between these domains matched the expectation for obverse/reverse twinning with the matrix ($\bar{1}00$; $0\bar{1}0$; 001). After integration with SAINT+, an absorption correction with TWINABS[28] based on multiple scans was applied. The structure solution by direct methods[29] was in full accord with the atomic coordinates as derived from powder diffraction. When only the major domain was considered, refinement with SHELXL[30] converged to residual values of $wR_2$ = 0.44 (all data) and $R_1$ = 0.20 and left a residual electron density of 32 e Å$^{-3}$. When obverse/reverse and inversion twinning in the noncentrosymmetric space group *R*3*m* (No. 160) was taken into account, these agreement factors improved to $wR_2$ = 0.24 (all data) and $R_1$ = 0.10, and the residual electron density decreased to 5 e Å$^{-3}$. In refining these intensity data, the more precise lattice parameters from the powder experiments were used.

Although the aforementioned domains could be assigned unambiguously, they cannot completely describe the diffraction pattern. This limitation is reflected in unsatisfactory residual values and the rather high residual electron-density maxima and minima. Together with In2, the most pronounced electron-density fluctuations in a final difference Fourier map are situated along the crystallographic *c* axis, at fractional coordinates of 0, 0, 0.140 (5.4 e Å$^{-3}$) and 0, 0, 0.074 (−8.6 e Å$^{-3}$). A view of these most relevant electron-density maxima and minima is provided in the Supporting Information. Less pronounced local electron-density fluctuations are encountered in the vicinity (0.6−0.9 Å) of the heavy atoms.

Tentative inclusion of additional smaller domains of the same compound caused less stable data integration and did not improve the refinement results. Additional details concerning the structure determination for 3R $In_2Se_3$ are available in CIF format and have been deposited under the CCDC entry number 1855522. Copies of the data can be obtained free of charge from CCDC.

The polycrystalline samples of 3R $In_2Se_3$ and crystals of 2H $In_2Se_3$ were mortared and measured by powder X-ray diffraction using a STADI MP diffractometer (STOE, Darmstadt, Germany) with monochromatic Mo K$\alpha_1$ radiation and a PSD detector. The intensity data were refined using the Fullprof program package.[31,32] Crystallographic and Rietveld refinement data are shown in Table 2. To

**Table 2. Rietveld Refinements of Powder XRD Data**

| | 2H $\alpha$-$In_2Se_3$ | 3R $\alpha$-$In_2Se_3$ |
|---|---|---|
| space group | $P6_3mc$ (No. 186) | *R*3*m* (No. 160) |
| *a* (Å) | 4.023(4) | 4.026(4) |
| *c* (Å) | 19.217(11) | 28.750(11) |
| *V* (Å$^3$) | 269.4(2) | 403.6(8) |
| *Z* | 2 | 3 |
| $\chi^2$ | 2.86 | 1.76 |
| $R_{Bragg}$ | 8.25 | 11.0 |
| $R_F$ | 8.47 | 8.12 |
| $R_p$ (%)[a] | 1.53 | 2.30 |
| $wR_p$ (%)[a] | 2.31 | 3.27 |

[a]Not corrected for background.

account for anisotropic broadening due to two-dimensional defects that could also be seen in the STEM images (see Figure S1), an anisotropic size model was employed while refining the diffraction pattern. For 3R $In_2Se_3$, the single-crystal data were used as a starting model with fixed atom sites and displacement parameters. For 2H $In_2Se_3$, due to a lack of single-crystal data, a starting model with quantum-chemically optimized atomic positions was used to refine the diffraction pattern. High-resolution XRD measurements at a synchrotron beamline are planned to fully refine the crystal structure. Both powder patterns show a reflection at 13.7° in 2Θ that might be indexed by $\beta$-$In_2Se_3$.

For TEM measurements, lamellas were produced by focused ion beam (FIB) technique employing an FEI Dual Beam Helios NanoLab system. The lamellas were cut along the *c* axis of $In_2Se_3$ single crystals.

The high-angle annular dark-field scanning transmission electron microscopy (HAADF-STEM) imaging together with STEM-energy dispersive X-ray spectroscopy (STEM-EDX) mappings were performed on an FEI Titan electron microscope, equipped with a Cs-aberration corrector for the probe-forming lens operated at 200/300 kV acceleration voltage. For EDX mapping a "Super-X" wide solid angle EDX detector was used at a voltage of 200 kV.

**Computational Details.** Density-functional theory (DFT) calculations employed the "D3" van der Waals correction[33] with dampening[34] on top of the PBE functional.[35] This approach reproduces structural parameters well and accounts for dispersion interactions between quintuple-layer blocks. We used plane-wave basis sets and the projector augmented wave (PAW) method[36] as implemented in the Vienna *Ab Initio* Simulation Package (VASP).[37−39] The energy cutoff for the plane-wave expansion was set to 500 eV with an electronic convergence criterion of $10^{-7}$ eV. Structural optimization was performed until residual forces fell below $1 \times 10^{-3}$ eV Å$^{-1}$. Reciprocal space was sampled on Γ-centered *k*-point grids with densities between 0.01 and 0.03 Å$^{-1}$ for structural relaxation. Chemical-bonding analyses of plane-wave data by Crystal Orbital Hamilton Population (COHP)[40,41] as well as Mulliken charge



DOI: 10.1021/acs.inorgchem.8b01950
Inorg. Chem. 2018, 57, 11775−11781

analysis were done using LOBSTER.[42−44] The following pseudopotentials have been employed: In, 4d, 5s, 5p; and Se, 4s, 4p.

## RESULTS

Figure 1 shows an HR HAADF-STEM image of two different polycrystalline $In_2Se_3$ samples. Because the intensity in

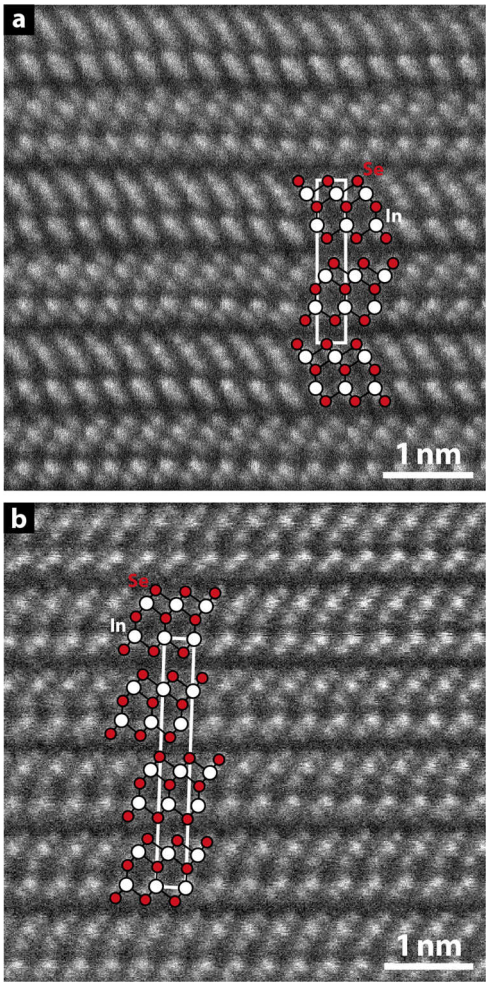


**Figure 1.** High-resolution HAADF-STEM *Z*-contrast images of (a) 2H and (b) 3R $In_2Se_3$ together with the structural models.

HAADF-STEM is roughly proportional to $Z^{1.8}$, this allows the straightforward interpretation of the images: In-rich columns appear slightly brighter than Se columns ($Z_{In}$ = 49, $Z_{Se}$ = 34). The results are confirmed by STEM-EDX mapping as shown in Figure S2. Thus, both samples are arranged in a layered structure of quintuple Se−In−Se−In−Se layer blocks stacked in one direction. The blocks are separated by van der Waals gaps.

The two In atoms in the layers are coordinated differently, one tetrahedrally and the other octahedrally. The difference between 2H and 3R $In_2Se_3$ lies in the stacking of these layers. The 2H and 3R $In_2Se_3$ structure models as created to fit the HAADF-STEM data were further optimized by quantum-chemical calculations and then used for refining powder XRD data. The 3R $In_2Se_3$ structure was confirmed by single-crystal diffraction.

Due to its layered van der Waals-like crystal structure, $\alpha$-$In_2Se_3$ shows a large number of two-dimensional defects perpendicular to its stacking in the bulk phase. This results in strong anisotropic broadening and preferred orientations in the PXRD data as visible in Figure 2.

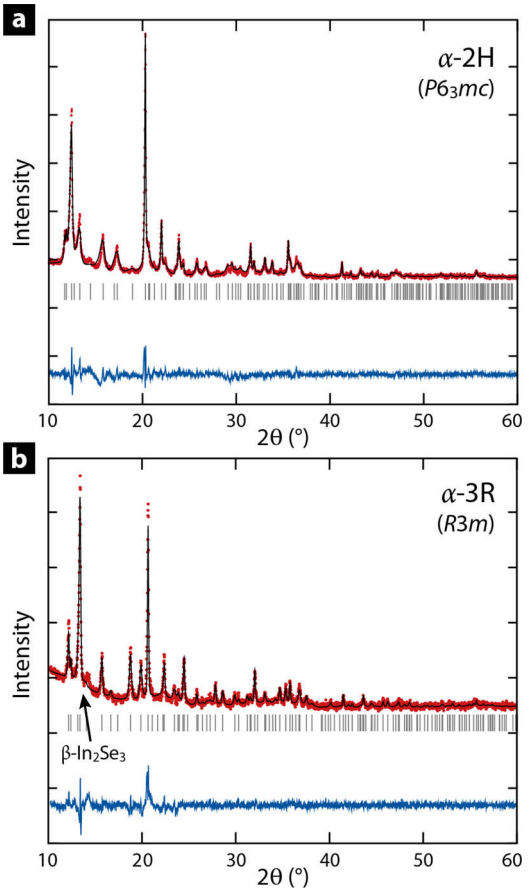


**Figure 2.** Refined X-ray powder diffraction patterns of (a) $\alpha$-2H and (b) $\alpha$-3R $In_2Se_3$ samples.

2H $In_2Se_3$ shows hexagonal symmetry with space group $P6_3mc$ and five different atomic sites (In1 on 2*a*, In2 on 2*b*, Se1 on 2*a*, Se2 on 2*b*, Se3 on 2*a*). Popovic et al. postulated space group $P6_3/mmc$ but without a structure model suggestion.[19] Each layer consists of two indium atoms with different coordination polyhedra: In1 is coordinated tetrahedrally by four Se atoms while In2 is octahedrally coordinated by six Se. Moving further, the 3R structure consists of identical quintuple layers in a different stacking. Instead of the "zigzag" motif of the 2H structure (see Figure 1a), the layers differ only on the basis of a translation along the *ab* plane. In 3R, five atomic sites (In1, In2, Se1, Se2, Se3; all on 3*a* positions) exist, arranged in a rhombohedral ($R3m$) crystal structure. By turning and moving the layers along the *ab* plane, both structures are easily transferred into each other.

A similar structure model for the 3R structure exists since 1966 and goes back to Osamura et al.,[45] who already described a quintuple-layer structure with $InSe_4$ tetrahedra and $InSe_6$ octahedra. The interatomic distances in their structure model, however, seem questionable, for example, homoatomic Se−Se distances of 2.61 Å in comparison to a heteroatomic In−Se distance of 3.51 Å. These questionable details by Osamura et al. probably go back to a simple printing mistake because their structure is close to ours if one exchanges the *z* parameters of Se2 and In1. Ye et al. suggested another layered structure with all tetrahedrally coordinated indium atoms.[46] However,



DOI: 10.1021/acs.inorgchem.8b01950
*Inorg. Chem.* 2018, 57, 11775−11781

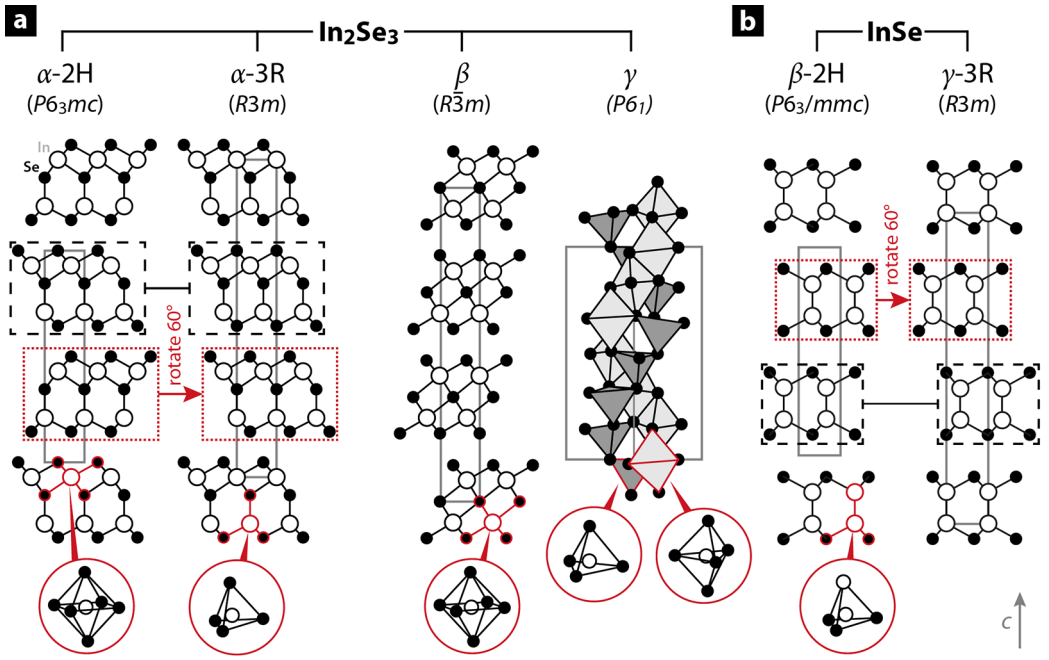


**Figure 3.** Projection of (a) $\alpha$-, $\beta$-, and $\gamma$-$In_2Se_3$ crystal structures and (b) stacking variants of $\alpha$-InSe along *c*, highlighting different coordination environments.

arranging quintuple Se−In−Se−In−Se layers with In atoms coordinated only tetrahedrally will result in some single-coordinated Se atoms. This is highly questionable already from chemical intuition, and DFT calculations show an instability of the all-tetrahedral coordination toward one octahedrally coordinated In atom. Almost 50 years later, in 2015, Debbichi et al.[23] postulated a new structure model for 3R $In_2Se_3$ by quantum-chemical calculations, which is isostructural to the structure found by our group. Very recently, Zhou et al. could experimentally confirm this very structure by electron microscopy of $In_2Se_3$ nanosheets.[9]

For 2H $In_2Se_3$, one structure model was already postulated by Semiletov in 1961,[47] also with all tetrahedrally coordinated In atoms. Like the 3R model from Ye et al., this model suffers from the single-coordinated selenium atoms. As mentioned before, however, a better model has recently been derived from electron microscopy results by Xue et al.[24]

Above 200 °C, $In_2Se_3$ is supposed to undergo a phase transition into $\beta$-$In_2Se_3$, which crystallizes in the $Bi_2Te_3$ structure type. This phase also consists of Se−In−Se−In−Se quintuple layers, but here, In is octahedrally coordinated throughout. $\beta$-$In_2Se_3$ is stable in nanosheets at room temperature[48] and was reported to be rapidly quenchable to room temperature as a bulk phase.[19] However, we were unable to reproduce this behavior.

Figure 3 displays the structural relationships between $\alpha$-, $\beta$-, and $\gamma$-$In_2Se_3$ as well as two stacking variants of indium monoselenide (InSe). The crystal structure of $\gamma$-$In_2Se_3$ is well-known and was solved by single-crystal refinement.[49] It crystallizes in a defect wurtzite type with vacancy spirals. This is the only known no-layered polymorph of $In_2Se_3$ and consist of tetrahedrally and pentagonally coordinated In atoms. In addition, there are two more potentially layered structures of $In_2Se_3$ reported in the literature: $\kappa$-$In_2Se_3$ crystallizes in nanosheets only and is supposed to be similar to the $\alpha$-phases,[50,51] while $\delta$-$In_2Se_3$ is a high-temperature phase stable above 720 °C[19] whose crystal structure is still unknown.

Indium monoselenide (InSe) also crystallizes in a layered structure but with quadruple Se−In−In−Se layers instead. Surprisingly, the polymorphism of InSe shows exactly the same stacking behavior as $\alpha$-$In_2Se_3$: one hexagonal stacking ($\beta$-InSe, $P6_3/mmc$), where every second layer is rotated by 60° around [001], and one rhombohedral stacking ($\gamma$-InSe, $R3m$), arranged by translation within the *ab* plane.

Heterointeratomic distances in the two $\alpha$-phases are very similar and range from 2.55 to 2.64 Å for the tetrahedrally coordinated In atom. For the octahedrally coordinated indium, the Se−In distances are larger, as expected (2.71−2.85 Å). These distances are in excellent agreement with those found in other compounds of the In−Se phase diagram, with similar coordination polyhedra. In $\gamma$-$In_2Se_3$ one In atom is also tetrahedrally coordinated with interatomic distances between 2.57 and 2.63 Å.[49] An $InSe_6$-octahedron can be found in the $In_6Se_7$ crystal structure, with In−Se distances of 2.65−2.89 Å.[52]

Given this overview of its structures, one may well ask why $In_2Se_3$ prefers a mixed coordination instead of an all-octahedral one. To answer this question, we performed bonding and charge analysis as will be discussed in the following.

Figure 4 shows Mulliken charges and projected COHP plots for $\alpha$-3R $In_2Se_3$ and $\beta$- and $\gamma$-$In_2Se_3$. The cationic indium charge within the structures varies from +0.40 to +0.52 e, with the $\beta$-phase being the least ionic of the three, while the $\alpha$-phase shows a slightly stronger cationic behavior of indium in the tetrahedral coordination. Interestingly, most electrons are transferred in the case of $\gamma$-$In_2Se_3$ where indium (within the strongly distorted tetrahedral or trigonal bipyramidal environments) has a charge of +0.50 to +0.52 e. Regarding the question from above, the ionic contributions of tetrahedrally coordinated In atoms are stabilizing the $\alpha$-phase when compared to the purely octahedral $\beta$-$In_2Se_3$.

Transitioning from ionic to covalent contributions we show COHP plots in Figure 4b. Here, stabilizing covalent interactions can be seen for the tetrahedrally coordinated In



DOI: 10.1021/acs.inorgchem.8b01950
*Inorg. Chem.* 2018, 57, 11775−11781

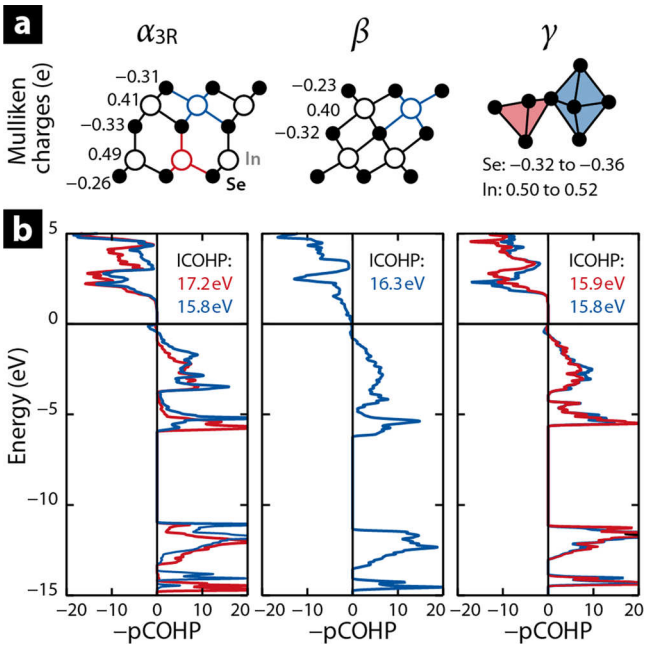


**Figure 4.** (a) Mulliken charges and (b) chemical-bonding analysis of selected $In_2Se_3$ polymorphs with bonding levels to the right and antibonding ones to the left. The colors of the COHP plot correspond to the bonds highlighted in the structural fragments shown above. Projected density of states (DOS) plots are provided in the Supporting Information.

atoms (in red) in the $\alpha$- and $\gamma$-phase. For such species, we observe no significant antibonding contributions below the Fermi level, which is contrasted by small antibonding contributions for the octahedrally coordinated atoms in the $\alpha$- and $\beta$-phase. Such antibonding regions are sometimes observed in chalcogenides used as PCMs[53] but are overall destabilizing and should be minimized. Furthermore, the integrated COHP values of 3R $In_2Se_3$ show us that the tetrahedral coordination is indeed favored by covalent interactions as analyzed within the COHP framework.

Hence, indium atoms within $In_2Se_3$ prefer a tetrahedral environment to an octahedral one both from a covalent as well as an ionic perspective. A purely tetrahedral environment, however, is not possible due to the stoichiometry of the compound, such that there results a proper mix of tetrahedral and octahedral sites as observed in diffraction and electron microscopy.

## CONCLUSION

By combining HR-HAADF STEM Z-contrast imaging, single-crystal and powder XRD, and also quantum-chemical calculations, we were able to identify the crystal structures of 2H and 3R $In_2Se_3$. These $\alpha$-phases of $In_2Se_3$ consist of quintuple Se−In−Se−In−Se layers with two distinct coordination environments for In, one tetrahedral and one octahedral. The two phases are stacking variants, which are selectively accessible by solid-state synthesis. The stability of tetrahedrally coordinated In atoms was elucidated using chemical-bonding analysis tools, which showed an increase in stability for covalent as well as ionic contributions when compared to $\beta$-$In_2Se_3$ with purely octahedral coordination.

## ASSOCIATED CONTENT

### Supporting Information

The Supporting Information is available free of charge on the ACS Publications website at DOI: 10.1021/acs.inorgchem.8b01950.

Atomic position for 2H and 3R $In_2Se_3$, HAADF-STEM Z-contrast image of 3R $In_2Se_3$, EDX mapping of Se and In in 2H $In_2Se_3$, location of the residual electron densities from single-crystal refinement, optical micrographs of polycrystalline samples of 3R and 2H $In_2Se_3$, and projected DOS of $\alpha_{3R}$-, $\beta$-, and $\gamma$-$In_2Se_3$ (PDF)

### Accession Codes

CCDC 1855522 contains the supplementary crystallographic data for this paper. These data can be obtained free of charge via www.ccdc.cam.ac.uk/data_request/cif, or by emailing data_request@ccdc.cam.ac.uk, or by contacting The Cambridge Crystallographic Data Centre, 12 Union Road, Cambridge CB2 1EZ, UK; fax: +44 1223 336033.

## AUTHOR INFORMATION


### Corresponding Author

*E-mail: drons@HAL9000.ac.rwth-aachen.de.

### ORCID

Michael Küpers: 0000-0002-8295-614X
Philipp M. Konze: 0000-0002-7946-702X
Alexander Meledin: 0000-0002-3200-0553
Joachim Mayer: 0000-0003-3292-5342
Ulli Englert: 0000-0002-2623-0061
Matthias Wuttig: 0000-0003-1498-1025
Richard Dronskowski: 0000-0002-1925-9624


### Notes

The authors declare no competing financial interest.

## ACKNOWLEDGMENTS

We acknowledge support by the Deutsche Forschungsgemeinschaft DFG (SFB 917 "Nanoswitches") and the Jülich-Aachen Research Alliance (JARA-HPC project jara0033). Moreover, the research leading to these results has received funding from the European Union Seventh Framework Programme (FP7/2007−2013) under grant agreement no. 340698.

## REFERENCES

(1) Almeida, G.; Dogan, S.; Bertoni, G.; Giannini, C.; Gaspari, R.; Perissinotto, S.; Krahne, R.; Ghosh, S.; Manna, L. Colloidal Monolayer $\beta$-$In_2Se_3$ Nanosheets with High Photoresponsivity. *J. Am. Chem. Soc.* **2017**, *139*, 3005−3011.

(2) Jacobs-Gedrim, R. B.; Shanmugam, M.; Jain, N.; Durcan, C. A.; Murphy, M. T.; Murray, T. M.; Matyi, R. J.; Moore, R. L.; Yu, B. Extraordinary Photoresponse in Two-Dimensional $In_2Se_3$ Nanosheets. *ACS Nano* **2014**, *8*, 514−521.

(3) Chen, S.; Liu, X.; Qiao, X.; Wan, X.; Shehzad, K.; Zhang, X.; Xu, Y.; Fan, X. Facile Synthesis of $\gamma$-$In_2Se_3$ Nanoflowers toward High Performance Self-Powered Broadband $\gamma$-$In_2Se_3$/Si Heterojunction Photodiode. *Small* **2017**, *13*, 1604033.

(4) Han, G.; Chen, Z.-G.; Drennan, J.; Zou, J. Indium Selenides: Structural Characteristics, Synthesis and Their Thermoelectric Performances. *Small* **2014**, *10*, 2747−2765.

(5) Yang, L.; Chen, Z.-G.; Dargusch, M. S.; Zou, J. High Performance Thermoelectric Materials: Progress and Their Applications. *Adv. Energy Mater.* **2018**, *8*, 1701797.

(6) Cui, J.; Peng, H.; Song, Z.; Du, Z.; Chao, Y.; Chen, G. Significantly Enhanced Thermoelectric Performance of $\gamma$-$In_2Se_3$



DOI: 10.1021/acs.inorgchem.8b01950
*Inorg. Chem.* 2018, 57, 11775−11781

through Lithiation via Chemical Diffusion. *Chem. Mater.* **2017**, *29*, 7467−7474.
(7) Ding, W.; Zhu, J.; Wang, Z.; Gao, Y.; Xiao, D.; Gu, Y.; Zhang, Z.; Zhu, W. Prediction of Intrinsic Two-Dimensional Ferroelectrics in $In_2Se_3$ and Other $III_2$-$VI_3$ van der Waals Materials. *Nat. Commun.* **2017**, *8*, 14956.
(8) Cui, C.; Hu, W.-J.; Yan, X.; Addiego, C.; Gao, W.; Wang, Y.; Wang, Z.; Li, L.; Cheng, Y.; Li, P.; Zhang, X.; Alshareef, H. N.; Wu, T.; Zhu, W.; Pan, X.; Li, L.-J. Intercorrelated In-Plane and Out-of-Plane Ferroelectricity in Ultrathin Two-Dimensional Layered Semiconductor $In_2Se_3$. *Nano Lett.* **2018**, *18*, 1253−1258.
(9) Zhou, Y.; Wu, D.; Zhu, Y.; Cho, Y.; He, Q.; Yang, X.; Herrera, K.; Chu, Z.; Han, Y.; Downer, M. C.; Peng, H.; Lai, K. Out-of-Plane Piezoelectricity and Ferroelectricity in Layered $\alpha$-$In_2Se_3$ Nanoflakes. *Nano Lett.* **2017**, *17*, 5508−5513.
(10) Choi, M. S.; Cheong, B.-k.; Ra, C. H.; Lee, S.; Bae, J.-H.; Lee, S.; Lee, G.-D.; Yang, C.-W.; Hone, J.; Yoo, W. J. Electrically Driven Reversible Phase Changes in Layered $In_2Se_3$ Crystalline Film. *Adv. Mater.* **2017**, *29*, 1703568.
(11) Rasmussen, A. M.; Teklemichael, S. T.; Mafi, E.; Gu, Y.; McCluskey, M. D. Pressure-Induced Phase Transformation of $In_2Se_3$. *Appl. Phys. Lett.* **2013**, *102*, 062105.
(12) Lee, H.; Kang, D.-H.; Tran, L. Indium Selenide ($In_2Se_3$) Thin Film for Phase-Change Memory. *Mater. Sci. Eng., B* **2005**, *119*, 196−201.
(13) Wuttig, M.; Yamada, N. Phase-Change Materials for Rewriteable Data Storage. *Nat. Mater.* **2007**, *6*, 824−832.
(14) Simpson, R. E.; Fons, P.; Kolobov, A. V.; Fukaya, T.; Krbal, M.; Yagi, T.; Tominaga, J. Interfacial phase-change memory. *Nat. Nanotechnol.* **2011**, *6*, 501−505.
(15) Thiel, A.; Koelsch, H. Studien über das Indium. *Z. Anorg. Chem.* **1910**, *66*, 288−321.
(16) Klemm, W.; Vogel, H. U. v. Messungen an Gallium- und Indium-Verbindungen. X. Über die Chalkogenide von Gallium und Indium. *Z. Anorg. Allg. Chem.* **1934**, *219*, 45−64.
(17) Hahn, H.; Frank, G. The Crystal Structure of $In_2Se_3$. *Naturwissenschaften* **1957**, *44*, 533.
(18) Miyazawa, H.; Sugaike, S. Phase Transition of $In_2Se_3$. *J. Phys. Soc. Jpn.* **1957**, *12*, 312.
(19) Popovic, S.; Tonejc, A.; Grzeta-Plenkovic, B.; Celustka, B.; Trojko, R. Revised and New Crystal Data for Indium Selenides. *J. Appl. Crystallogr.* **1979**, *12*, 416−420.
(20) Likforman, A.; Fourcroy, P.-H.; Guittard, M.; Flahaut, J.; Poirier, R.; Szydlo, N. Transitions de la Forme de Haute Température $\alpha$ de $In_2Se_3$, de Part et d'Autre de la Température Ambiante. *J. Solid State Chem.* **1980**, *33*, 91−97.
(21) Lutz, H. D.; Fischer, M.; Baldus, H. P.; Blachnik, R. Zur Polymorphie des $In_2Se_3$. *J. Less-Common Met.* **1988**, *143*, 83−92.
(22) Vilaplana, R.; Parra, S. G.; Jorge-Montero, A.; Rodríguez-Hernández, P.; Munoz, A.; Errandonea, D.; Segura, A.; Manjón, F. J. Experimental and Theoretical Studies on $\alpha$-$In_2Se_3$ at High Pressure. *Inorg. Chem.* **2018**, *57*, 8241−8252.
(23) Debbichi, L.; Eriksson, O.; Lebegue, S. Two-Dimensional Indium Selenides Compounds: An Ab Initio Study. *J. Phys. Chem. Lett.* **2015**, *6*, 3098−3103.
(24) Xue, F.; Zhang, J.; Hu, W.; Hsu, W.-T.; Han, A.; Leung, S.-F.; Huang, J.-K.; Wan, Y.; Liu, S.; Zhang, J.; He, J.-H.; Chang, W.-H.; Wang, Z. L.; Zhang, X.; Li, L.-J. Multidirection Piezoelectricity in Mono- and Multilayered Hexagonal $\alpha$-$In_2Se_3$. *ACS Nano* **2018**, *12*, 4976−4983.
(25) Schäfer, H. *Chemische Transportreaktionen*; Verlag Chemie: Weinheim, Germany, 1962.
(26) Binnewies, M.; Glaum, R.; Schmidt, M.; Schmidt, P. *Chemische Transportreaktionen*; de Gruyter: Berlin, Germany, 2011.
(27) Sheldrick, G. M. *CELL_NOW*; University of Göttingen: Germany, 2009.
(28) Sheldrick, G. M. *TWINABS*; University of Göttingen: Germany, 2008.
(29) Sheldrick, G. M. A short history of SHELX. *Acta Crystallogr., Sect. A: Found. Crystallogr.* **2008**, *64*, 112−122.
(30) Sheldrick, G. M. Crystal structure refinement with SHELXL. *Acta Crystallogr., Sect. C: Struct. Chem.* **2015**, *71*, 3−8.
(31) Rodríguez-Carvajal, J. Recent advances in magnetic structure determination by neutron powder diffraction. *Phys. B* **1993**, *192*, 55−69.
(32) Rodríguez-Carvajal, J., Recent developments of the program FULLPROF. *Commission on Powder Diffraction (IUCr) Newsletter* **2001**, *26*, 12−19.
(33) Grimme, S.; Antony, J.; Ehrlich, S.; Krieg, H. A Consistent and Accurate *ab initio* Parametrization of Density Functional Dispersion Correction (DFT-D) for the 94 Elements H-Pu. *J. Chem. Phys.* **2010**, *132*, 154104.
(34) Grimme, S.; Ehrlich, S.; Goerigk, L. Effect of the damping function in dispersion corrected density functional theory. *J. Comput. Chem.* **2011**, *32*, 1456−1465.
(35) Perdew, J. P.; Burke, K.; Ernzerhof, M. Generalized Gradient Approximation Made Simple. *Phys. Rev. Lett.* **1996**, *77*, 3865−3868.
(36) Blöchl, P. E. Projector Augmented-Wave Method. *Phys. Rev. B: Condens. Matter Mater. Phys.* **1994**, *50*, 17953−17979.
(37) Kresse, G.; Furthmüller, J. Efficient Iterative Schemes for Ab Initio Total-Energy Calculations Using a Plane-Wave Basis Set. *Phys. Rev. B: Condens. Matter Mater. Phys.* **1996**, *54*, 11169−11186.
(38) Kresse, G.; Furthmüller, J. Efficiency of ab-initio Total Energy Calculations for Metals and Semiconductors Using a Plane-Wave Basis Set. *Comput. Mater. Sci.* **1996**, *6*, 15−50.
(39) Kresse, G.; Joubert, D. From Ultrasoft Pseudopotentials to the Projector Augmented-Wave Method. *Phys. Rev. B: Condens. Matter Mater. Phys.* **1999**, *59*, 1758−1775.
(40) Crystal Orbital Hamilton Population (COHP) analysis is a chemical-bonding tool based on a partitioning technique of the band-structure energy, that is, the sum of the Kohn−Sham eigenvalues. Its energy integral (ICOHP) up to the Fermi level serves as a quantitative measure of covalent bond strength.
(41) Dronskowski, R.; Blöchl, P. E. Crystal Orbital Hamilton Populations (COHP). Energy-Resolved Visualization of Chemical Bonding in Solids Based on Density-Functional Calculations. *J. Phys. Chem.* **1993**, *97*, 8617−8624.
(42) Deringer, V. L.; Tchougréeff, A. L.; Dronskowski, R. Crystal Orbital Hamilton Population (COHP) Analysis As Projected from Plane-Wave Basis Sets. *J. Phys. Chem. A* **2011**, *115*, 5461−5466.
(43) Maintz, S.; Deringer, V. L.; Tchougréeff, A. L.; Dronskowski, R. Analytic Projection from Plane-Wave and PAW Wavefunctions and Application to Chemical-Bonding Analysis in Solids. *J. Comput. Chem.* **2013**, *34*, 2557−2567.
(44) Maintz, S.; Deringer, V. L.; Tchougréeff, A. L.; Dronskowski, R. LOBSTER: A Tool to Extract Chemical Bonding from Plane-Wave Based DFT. *J. Comput. Chem.* **2016**, *37*, 1030−1035.
(45) Osamura, K.; Murakami, Y.; Tomiie, Y. Crystal Structures of $\alpha$- and $\beta$-Indium Selenide, $In_2Se_3$. *J. Phys. Soc. Jpn.* **1966**, *21*, 1848.
(46) Ye, J.; Soeda, S.; Nakamura, Y.; Nittono, O. Crystal Structures and Phase Transformation in $In_2Se_3$ Compound Semiconductor. *Jpn. J. Appl. Phys., Part 1* **1998**, *37*, 4264−4271.
(47) Semiletov, S. A. Crystal Structure of the Low-Temperature Modification of $In_2Se_3$. *Sov. Phys. Crystallogr.* **1961**, *6*, 158−160.
(48) Tao, X.; Gu, Y. Crystalline−Crystalline Phase Transformation in Two-Dimensional $In_2Se_3$ Thin Layers. *Nano Lett.* **2013**, *13*, 3501−3505.
(49) Pfitzner, A.; Lutz, H. D. Redetermination of the Crystal Structure of $\gamma$-$In_2Se_3$ by Twin Crystal X-Ray Method. *J. Solid State Chem.* **1996**, *124*, 305−308.
(50) Jasinski, J.; Swider, W.; Washburn, J.; Liliental-Weber, Z.; Chaiken, A.; Nauka, K.; Gibson, G. A.; Yang, C. C. Crystal Structure of $\kappa$-$In_2Se_3$. *Appl. Phys. Lett.* **2002**, *81*, 4356−4358.
(51) Li, Y.; Gao, J.; Li, Q.; Peng, M.; Sun, X.; Li, Y.; Yuan, G.; Wen, W.; Meyyappan, M. Thermal Phase Transformation of $In_2Se_3$ Nanowires Studied by in situ Synchrotron Radiation X-Ray Diffraction. *J. Mater. Chem.* **2011**, *21*, 6944−6947.


DOI: 10.1021/acs.inorgchem.8b01950
*Inorg. Chem.* 2018, 57, 11775−11781

(52) Walther, R.; Deiseroth, H. J. Redetermination of the Crystal Structure of Hexaindium Heptaselenide, $In_6Se_7$. *Z. Kristallogr.* **1995**, *210*, 359.
(53) Wuttig, M.; Lüsebrink, D.; Wamwangi, D.; Wełnic, W.; Gilleßen, M.; Dronskowski, R. The role of vacancies and local distortions in the design of new phase-change materials. *Nat. Mater.* **2007**, *6*, 122−128.



DOI: 10.1021/acs.inorgchem.8b01950
*Inorg. Chem.* 2018, 57, 11775−11781